J. Fluid Mech. (1973), *vol.* 60, *part* 3, *pp.* 539–559
Printed in Great Britain

Heat-flux transitions at low Rayleigh number

By WENDELL BROWN

Department of Meteorology, Massachusetts Institute of Technology†

(Received 9 November 1971 and in revised form 16 May 1973)

The transition to turbulence in the convective flow of air between horizontal plates in a circular convection chamber has been investigated. Measurements of the heat flux and the instantaneous spatial temperature field were made simultaneously for a range of Rayleigh number Ra between 3×10^3 and 5×10^4. Ra could be varied by changing the vertical separation or the temperature difference between the plates. The temperature field was measured with either a horizontal or a vertical array of resistance wires mounted so that the flow field could be traversed at velocities much greater than flow velocities characteristic of thermal convection. Slope transitions in the heat flux were found at $Ra = 9600$ and $Ra = 26000$. Many measurements of the instantaneous horizontal distribution of temperature for $Ra > Ra_{T2}$ indicate a growth in amplitude of fluctuations with non-dimensional cyclical wavenumbers of 0·4 and greater. The probability of observing these high wavenumber fluctuations also increases as Ra becomes greater than Ra_{T2}. The horizontal wavelengths of the different types of temperature fluctuations are compared with the observations of others.

1. Introduction

The sequence of states that a rigidly bounded convective flow field passes through is characteristic of what is defined in the literature as a slow transition to turbulence. Coles (1965) notes 'a transition by spectral evolution' in connexion with his observation of the instabilities in circular Couette flow. This type of transition generally can be associated with hydrodynamic flow fields where the characteristic parameter (e.g. the Reynolds number, the Taylor number or the Rayleigh number) is constant throughout the flow field. This type of transition is a contrast to the 'fast' transitions which occur in boundary-layer flow, where the Reynolds number varies with position. Flows that undergo slow transitions are the popular candidates for laboratory investigations because each event of the series that leads to turbulence can be more easily isolated.

An experimental investigation of convection by Malkus (1954) showed that the slope of the heat-flux relation was marked by several discontinuities at various Rayleigh numbers Ra_{Ti}; $i = 2, 3, \ldots$. The work of Willis & Deardorff (1967) confirmed some of the heat-flux transitions. Those experiments, performed in a rectangular geometry with air and silicone oil ($Pr = 57$), exhibited slope

† Present address: Institute of Geophysics and Planetary Physics, University of California, La Jolla, California 92037.

discontinuities for Ra as high as $2{\cdot}8 \times 10^6$, which is well into the so-called 'turbulent' regime. A series of experiments performed by Krishnamurti (1970) disagrees with Willis & Deardorff's (1967) conclusion that the Ra_{T_i} are independent of Pr. A correlation of photographs of the evolving convection roll structure and simultaneous heat-flux measurements shows that high Pr fluids become unstable to three-dimensional disturbances at the second heat-flux transition at $Ra_{T_2} \simeq 20\,000$. The more recent observations of Busse & Whitehead (1971) and Willis, Deardorff & Somerville (1972) confirm this gradual onset of the bimodal mode. At a higher Ra Krishnamurti reports that the three-dimensional cells become time dependent and at a still higher Ra the fluid becomes turbulent.

Other experimental results show us other characteristics of convection. Koschmieder's (1966) pictures of concentric rolls in a circular tank and Krishnamurti's (1970) observations of rectangular-box convection are persuasive evidence of the importance of the lateral boundaries in determining the roll orientation for fluids with $Pr > 6{\cdot}7$ (water). Willis & Deardorff (1970) present pictures of low Ra convection that are very helpful in interpreting the temperature-field data obtained in these experiments. These photographs show that rolls are the dominant mode of flow for $Ra < 10\,000$ and that the flow exhibits two types of time-dependent flow for some regimes of Ra. The first type is a lateral wave superposed most often on the straighter rolls for $Ra > 5800$. Their study shows quite conclusively that it is this class of motion that explains the unsteadiness reported by many investigators measuring temperature at a stationary point in the flow field.

It is the results of the experiments performed by Malkus and Willis & Deardorff that have motivated this investigation, whose aim is to answer questions about the discontinuities in the rate of change of the heat flux with Ra in air. The details of the disagreement of Krishnamurti's results with the results of Malkus and Willis & Deardorff about the Prandtl number dependence of the discontinuities remain to be studied more thoroughly. A detailed study of the role of Pr in transition to turbulent convection could reveal important differences in the convective dynamics associated with air, for which Pr is near 1.

The parameters one uses to describe convective heat transfer can be found by combining the boundary conditions and Boussinesq equations of motion in non-dimensional form. The only parameters governing the dynamics of this model are the resulting dimensionless groups, which are used as a basis for comparing experimental results. It has been shown by many authors that the Rayleigh number and the Prandtl number are the parameters that govern the dynamics in a Boussinesq system in which fluid properties are constant. They are defined thus:

$$Ra = \alpha g \Delta T h^3 / \kappa \nu, \quad Pr = \nu / \kappa,$$

where α is the coefficient of volumetric expansion, g is the gravitational acceleration, ΔT and h are the temperature difference and distance, respectively, between the upper and lower boundaries, ν is the kinematic viscosity coefficient and $\kappa \equiv K/\rho C_p$ is the thermal diffusivity, where ρ is density, C_p is the constant-

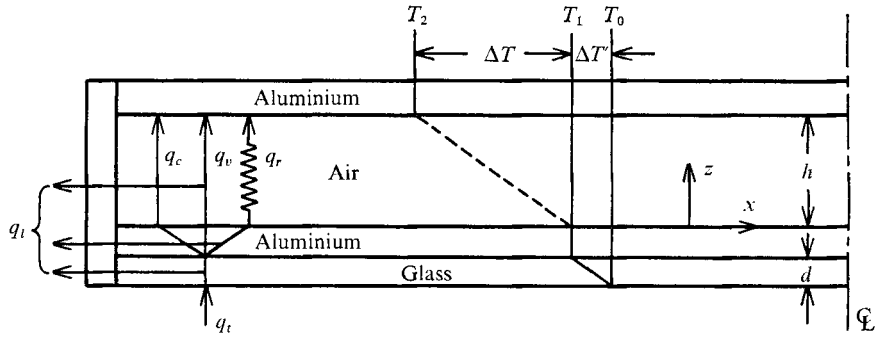

FIGURE 1. Schematic diagram of thermal convection for $Ra < 50\,000$ in air. The horizontal mean temperature distribution is shown to the right of heat-flux components; q_c, conductive; q_v, convective; q_r, radiative; q_l, heat losses.

pressure specific heat and K is the thermal conductivity. The dimensionless heat transport is defined in terms of the Nusselt number

$$Nu = -\frac{h}{\Delta T}\frac{d\bar{T}}{dz}\bigg|_{z=0},$$

which is just an expression of the ratio of the sum of convected plus conducted heat flux through the fluid to the heat flux due to conduction alone. Figure 1 is a schematic diagram showing the parameters associated with the convection that is to be discussed.

2. Description of apparatus

Two 1·27 cm aluminium plates formed the upper and lower boundaries of the 74 cm diameter convection chamber,† pictured in figure 2. The heat flux from the lower to upper plate was inferred from the temperature across a 0·925 cm thick glass plate adjacent to the lower plate. A circular Plexiglas–stryrofoam insulation ring sealed the working fluid, which was air in this case, from the laboratory environment.

The upper plate was secured in its horizontal position by an overhead framework, while the lower glass–aluminium plate sandwich rested in a shallow pan mounted on a movable vertical shaft. In these experiments plate separations up to 7 cm were readily attained. The upper plate was levelled with respect to the lower plate assembly, which could be floated in cerrobend (a lead–bismuth alloy whose melting-point = 73 °C), which also served as an excellent thermal buffer for the lower plate. Excellent temperature control was maintained by two constant-temperature baths above and below the boundaries respectively. Temperature differences ΔT as large as 30 °C centred at room temperature could be maintained to within $\pm 0{\cdot}01$ °C. A radial array of thermocouples was used to check for unsatisfactory radial temperature gradients.

† A more detailed description can be found in Brown (1971).

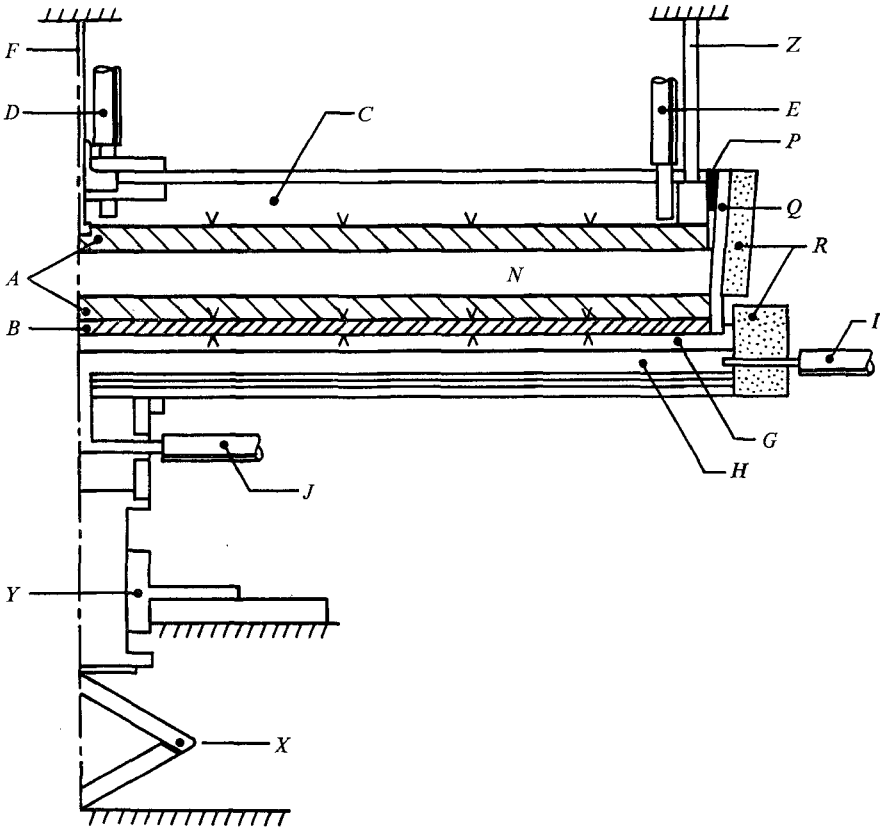

FIGURE 2. Schematic diagram of the convection chamber. A, upper and lower boundaries; B, glass plate, 0·925 cm thick; C, D, E, cooling-water chamber, inlet, and outlet, respectively; F, sag adjustment screw; G, woods metal, lead–bismuth alloy, density = 9 g/cm^3; H, I, J, heating-water chamber, inlet, and outlet, respectively, aluminium top and bottom, 1·27 cm thick, resting on asbestos; N, air filled convection chamber; P, inner tube; Q, Plexiglas outer wall (attached to bottom plate); R, insulation; X, support jack to adjust spacing; Y, sleeve bearing for vertical alignments, 10 cm diameter; Z, support rods; $\vee$, $\wedge$, thermocouple locations; plate diameter = 74 cm.

Constant-current resistance wire temperature sensors were used in a four-probe horizontal array (figure 3) to measure the spatial temperature field. These probes were mounted on an assembly that was supported by a pair of teflon runners which rode on the upper and lower plates. This assembly was projected into the tank on the end of a long shaft secured to the horizontal driving traverse. For these experiments typical speeds of about 25 cm/s were constant over 80 % of the 64 cm run.

3. Heat-flux measurements

It is especially important when comparing features of convection at low Ra that the calculation of Ra and Pr be discussed. Since the quantities κ and ν are temperature dependent, an average value (i.e. that associated with the mean

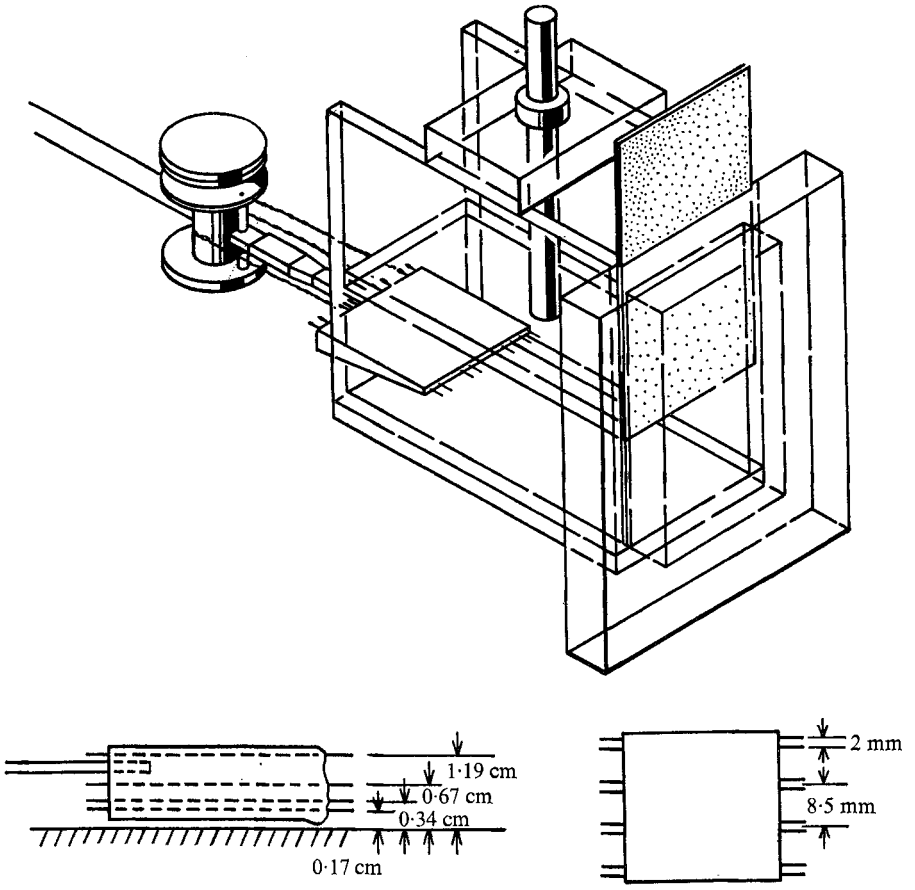

FIGURE 3. Vertical and horizontal arrays used to measure horizontal temperature distribution. The array and support are poised near the entrance chute, which is attached to the side of the convection tank. The 2 mm sensor elements are separated by 8·5 mm on the horizontal array and as shown on the vertical array.

Temperature (°C)	ν ($cm^2 s^{-1} \times 10^2$)	κ ($cm^2 s^{-1} \times 10^2$)	$Pr = \nu/\kappa$
−23·3	9·50	13·18	0·720
26·7	15·90	22·20	0·716
76·6	20·80	29·81	0·698

TABLE 1. Kinematic viscosity and thermal diffusivity of dry air at sea level (*National Bureau of Standard Circular*, no. 564)

tank temperature) was used for the calculation. In this case their values were determined from a linear interpolation of the values in table 1. If air is assumed to be a perfect gas the value of α is just the reciprocal of the mean absolute temperature. The measurement uncertainty of both the plate separation h and the unstable temperature difference ΔT between the two plates contributed to most of the error in the determination of Ra.

One of the versatile features of the apparatus is the variability of the plate separation. However, care must be taken in order to ensure both that the plates

are kept parallel and that the separation is measured accurately. The first requirement can be satisfied by floating the lower plate assembly in molten cerrobend and aligning the upper plate with the lower. Three-gauge blocks equidistantly positioned in the middle of the chamber were used as guides when aligning the plates. This was accomplished by adjusting the three threaded supports on the perimeter of the upper thermal bath and the sag compensation screw in the centre. If the cooling rate of the cerrobend was slow ($< 20\,°C/h$) no detectable distortion in the parallel plate separation was observed.

Accurate measurements of the plate separation to within $\pm 0{\cdot}0004$ cm were achieved by using a depth micrometer that was inserted through the vertical probe guide into the chamber. The three separate probe guide holes were used to monitor the parallax of the plates as either the gap or temperature difference between the plates was changed. The sum of measurement uncertainty, parallax and plate waviness produced uncertainties in the determination of h less than $\pm 1{\cdot}25\,\%$ for $h > 1$ cm.

For each of the experiments to be discussed the individual e.m.f. of each thermocouple was measured, yielding a well-documented history of plate temperature distribution over a wide variety of boundary conditions. For isothermal conditions the output e.m.f. of individual thermocouples varied by no more than $1\,\mu V$ ($0{\cdot}0164\,°C$) over $30{\cdot}5$ cm of the chamber radius of 37 cm. The observed radial temperature gradient for departure from isothermal conditions was related so closely to the difference between the plate and ambient temperature that the variation of the temperature difference ΔT over the inner 80 % of the chamber was less than 1 % for $\Delta T > 5°$. An uncertainty in the mean ΔT of $\pm 0{\cdot}06\,°C$ resulted from the scatter associated with the thermocouple calibrations.

In all but a few of the experiments discussed here the uncertainties in h and ΔT discussed imply an uncertainty in the determination of the Ra of less than 6 %. It was an unusual experiment for which $h < 1$ cm and/or $\Delta T > 25\,°C$, and for those cases a precise determination of Ra was not crucial.

The determination of Nu is a matter of finding the ratio of the sum of the convected and conducted heat fluxes, q_v and q_c respectively, and the conducted heat flux alone. This can be represented as follows:

$$Nu - 1 = q_v/q_c.$$

It is q_c and q_v that were calculated from experimental measurements using equations which are discussed in the appendix. The precision of the heat-flux measurements is indicated by figure 4, which shows how well two sets of data from these experiments compare with those found from Silveston's (1958) detailed experiments. Within the limits of experimental error all data agree with the prediction of $Ra = 1708$ found from linear analysis.

The primary aim of this investigation is to study in detail the discontinuities in the slope of the relation between the heat flux and the Rayleigh number. Because there are disagreements in the literature about the number and Ra of these discontinuities several series of heat-flux measurements for

$$500 < Ra < 50\,000$$

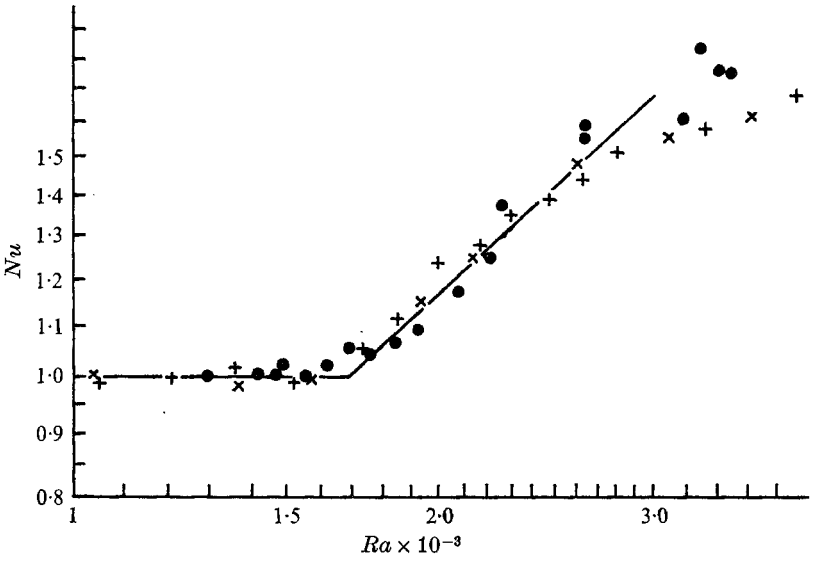

FIGURE 4. Heat flux at Ra near the value for onset of convection, $Ra_{cr} = 1710 \pm 40$. ×, +, present results, $Pr = 0{\cdot}71$; ●, Silveston's measurements, $Pr = 6{\cdot}7$.

were made. Since Ra could be varied in the apparatus by changing either the temperature difference or plate separation independently, both types of heat-flux experiment were performed. An experimental series in which Ra was varied by ΔT changes only (constant h) will be referred to as a $\delta\Delta T$ series, while its counterpart involving h changes (constant ΔT) will be referred to as a δh series.

All experiments were performed under steady-state conditions compared with the slowly varying experiments of Willis & Deardorff (1967) and Malkus (1954). Measurements were made at least 30 min after the variations in the differential e.m.f. across the glass plate had become smaller than the resolution of the Northrup K-3 potentiometer ($\pm 0{\cdot}75\,\mu$V or $\pm 0{\cdot}01\,^{\circ}$C).

4. Temperature-distribution measurements

A major concern is the disturbance field generated by the traversing probe. In order to minimize the disturbance field at the sensing wires of the probe, the sensing wires were mounted on a slender support and placed 7 cm ahead of the guide assembly. The probe was traversed near a stationary temperature probe which had the same time response characteristics as the moving probe sensors. For $\Delta T < 30\,^{\circ}$C and $Ra < 7000$ no disturbance was detectable at the stationary probe before the moving probe was past it. In fact, by a fortuitous accident, the moving probe once hit the stationary probe, establishing the time of passage with precision. No signal disturbance was detected at the stationary probe before it broke.

The decay of the disturbance field generated by the probe was assessed by waiting for varying periods between probe withdrawal and the next injection. An upper bound for the time constant for the decay of a perturbation of the

Series	Array†	Non-dimensional probe height	Mean temperature (°C)	$\delta\Delta T$ series Range (°C)	$\delta\Delta T$ series h (cm)	δh series Range (cm)	δh series ΔT (°C)	$Ra \times 10^{-3}$ range
I	H	0·05–0·28 Various	60–45	5·0–37·0	2·01	—		4·3–24·5
II	V	0·05‡	60–45	5·0–37·0	2·01	—		4·3–24·5
III§	H	0·25	~ 25	5·0–19·5	1·95	—		3·9–13·9
IV§	H	0·20	~ 25	5·0–27·1	2·73	—		9·8–53·4
V§	H	0·28	~ 25	9·1–28·9	1·67	—		3·9–12·0
VI§	H	0·29–0·32	~ 25	—		1·58–1·73	21·0	7·9–10·6
VII§	H	0·24–0·49	~ 25	—		1·60–3·03	20·3	7·3–54·0
VIII	V	0·03–0·12‡	~ 36	—		1·40–6·05	50·0	11·0–760·0

† H, horizontal array; V, vertical array.
‡ Probe nearest the lower plate.
§ Coincident heat-flux measurements.

TABLE 2. Summary of experimental conditions for temperature fluctuation runs

convecting fluid was also estimated. Because the Prandtl number of air is near unity, the viscous and thermal diffusion scales are comparable, so no distinctions need to be made. From the work of Chen & Whitehead (1968) the time scale T of a horizontal propagating disturbance is $N\tau_0$, where τ_0 is the mean orbital period of a particle in a convective roll and N the number of such rolls in the apparatus. For the conditions in our apparatus, a typical orbital velocity of 1·5 cm/s (the orbital period $\tau_0 = 5{\cdot}5$ s) was estimated from the numerical results of Chorin (1967) (with $Pr = 1$, $h = 2$ cm). For $N = 20$ a typical time scale of decay is therefore of order 120 s for $Ra > 10^4$. We chose to wait 10 min or five time constants between runs. Successive runs more than 5 min apart showed no detectable influence and did not differ from runs made after the apparatus had been left undisturbed for hours. The use of the trap door and probe chute was probably a crucial feature in the prevention of external influences both on the flow and its recovery from disturbances.

After the existence of three discontinuities in the slope of the heat-flux curve had been confirmed, a study of the temperature fields associated with the discontinuities was made. A measurement of the temperature distribution in the convecting flow field was made with the resistance wire temperature sensors. The horizontal array was used to measure the wavenumber field of the motions and the relative orientation of certain features of the flow field, while variations in the vertical structure of the temperature field were measured by the vertical array. Preliminary temperature measurements (I and II in table 2) with both types of arrays indicated that the horizontal array would provide the most important information about the changes in the instantaneous temperature field. The measurements with the vertical array provided information necessary to compare temperature fluctuations at different distances from the plates.

A typical series of temperature fluctuation measurements was designed to span a range of Ra between transition Rayleigh numbers. The plate separation

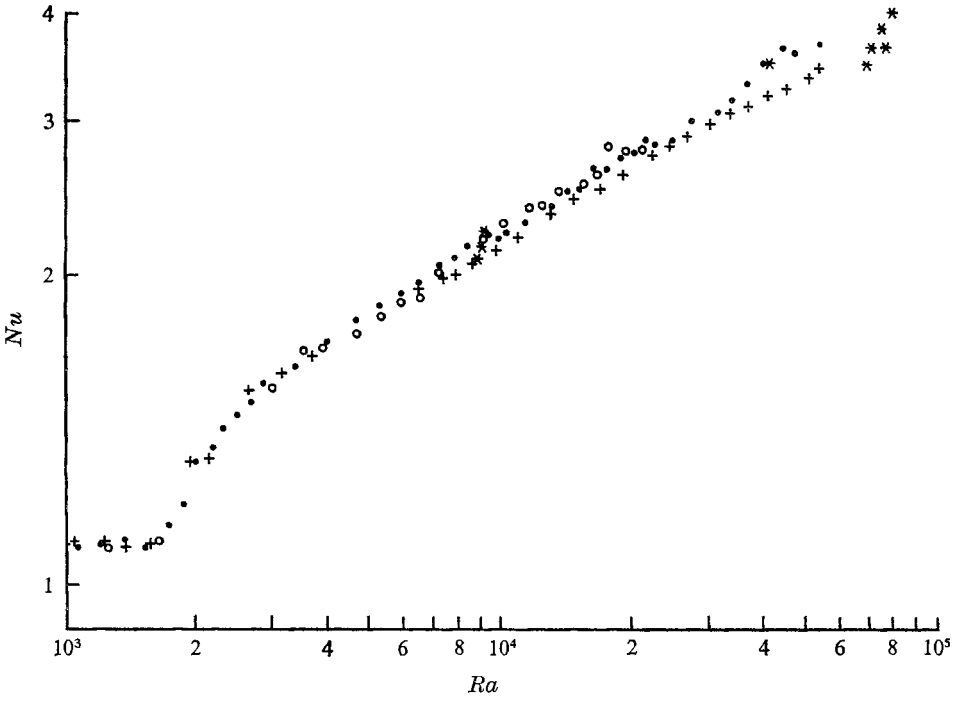

FIGURE 5. Summary of the heat-flux experiments. ○, $\Delta T = 24{\cdot}28\,^{\circ}\mathrm{C}$, $T_m = 50{\cdot}98\,^{\circ}\mathrm{C}$; ●, $\Delta T = 19{\cdot}70\,^{\circ}\mathrm{C}$, $T_m = 53{\cdot}20\,^{\circ}\mathrm{C}$; +, $\Delta T = 20{\cdot}30\,^{\circ}\mathrm{C}$, $T_m = 25{\cdot}03\,^{\circ}\mathrm{C}$; ⁎, after Mull & Reiher in air.

for a particular $\delta\Delta T$ series was usually chosen so that the maximum temperature difference ΔT occurred at the highest Ra of interest. We were restricted by the probe size to a minimum plate separation of 1·5 cm. Table 2 summarizes the different series of temperature fluctuation measurements. On the basis of observations of the temperature fluctuations measured at $Ra < 50000$, a final series of runs probing the mean temperature boundary layer was made for $Ra > 10^5$. The vertical array was chosen to investigate further the evolution and role of three-dimensional structures observed intermittently at the lower Ra. A detailed discussion of those results appears in Brown (1971).

5. Heat-flux results

The results of three separate series of heat-flux measurement are combined in figure 5. For these series Ra was varied by changing h while ΔT remained constant. The different sets of heat-flux measurements for Ra near Ra_{cr} are consistent among themselves and show excellent agreement with the highly regarded results of Silveston (1958) for $Ra < 2500$. The individual series show a systematic spreading of Nu for higher Ra. This is attributed to additional heat losses that occurred for the series with the greater mean temperatures. These additional heat losses are unaccounted for in the heat-flux calculation (see appendix). The air heat-flux data presented by Mull & Reiher (after Schmidt & Milverton 1935) are consistent

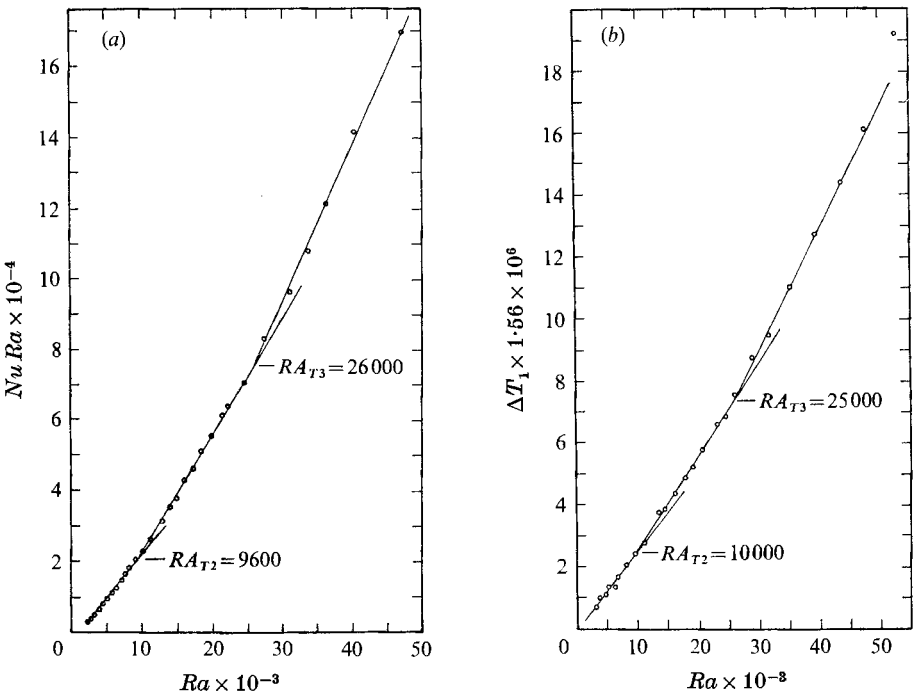

FIGURE 6. Heat flux for (*a*) a δh series, exhibiting slope transitions at $Ra = 9600$ and $Ra = 26000$, and (*b*) a δT series, exhibiting slope transitions at $Ra = 10000$ and $Ra = 25000$.

with the results found here. A comparison of our results with those of Willis & Deardorff (1967) tends to confirm their suspicisions that they may have made a 10 % underestimate in the determination of the heat flux.

Like the results of Willis & Deardorff (1967), the heat-flux measurements shown in figure 6 exhibit transitions at Ra near 10000 and 25000. Also no hysteresis of the slope discontinuity at Ra_{T2} was observed for experiments performed by both increasing and decreasing Ra. The fact that these transitions are essentially aspect-ratio independent for $D/h > 20$, where D is the chamber diameter, is shown in figure 6. This is an example of heat-flux measurements from both a δh series and a $\delta \Delta T$ series. Slope transitions near $Ra = 10^4$ and $2{\cdot}5 \times 10^4$ are clearly evident in both sets of measurements. It follows that comparisons between measurements from both δh and $\delta \Delta T$ series should be meaningful.

6. Results of the temperature-field investigation

Representative measurements of the horizontal temperature distribution made at $Ra > Ra_{T2}$ are shown in figures 7 (*a*) and (*b*) along with the isotherms and autospectra of the temperature fluctuations. These particular examples show how the temperature signature varies with a change of roll orientation relative to the direction of the probe. The axis of the main roll structure may be inferred from the orientation of the regions of maximum (cross-hatched) and minimum

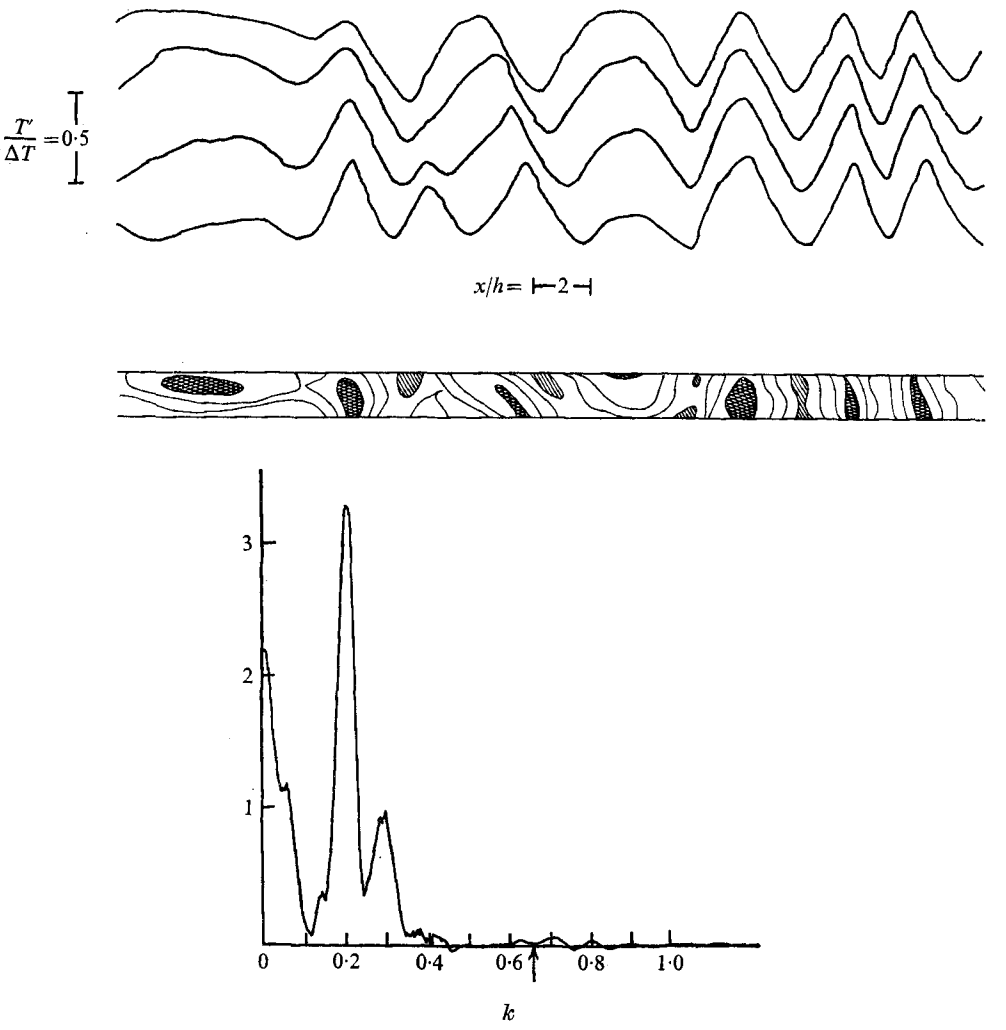

FIGURE 7 (*a*). For legend see p. 550.

(singly hatched) temperature. A typical measurement of the vertical distribution of horizontal temperature fluctuations is shown in figure 8. It demonstrates that at these low Ra there is no significant change in the appearance of the fluctuations at different non-dimensional heights Z_i^* above the plate.

A description of the temperature field for $Ra > Ra_{T2}$ is more complex and is summarized in figure 9 by a set of representative temperature measurements made at $Ra = 12 \times 10^3$. The time dependence of the flow field is obvious. The types of temperature fluctuation signatures recorded showed no preferred sequence while Ra was constant. Most measurements had a broader band appearance like those shown in figures 9 (*a*) and (*b*). However, occasionally at all Ra between Ra_{T2} and Ra_{T3} one observes a more uniform temperature distribution such as that shown in figure 9 (*c*). The most obvious difference between the

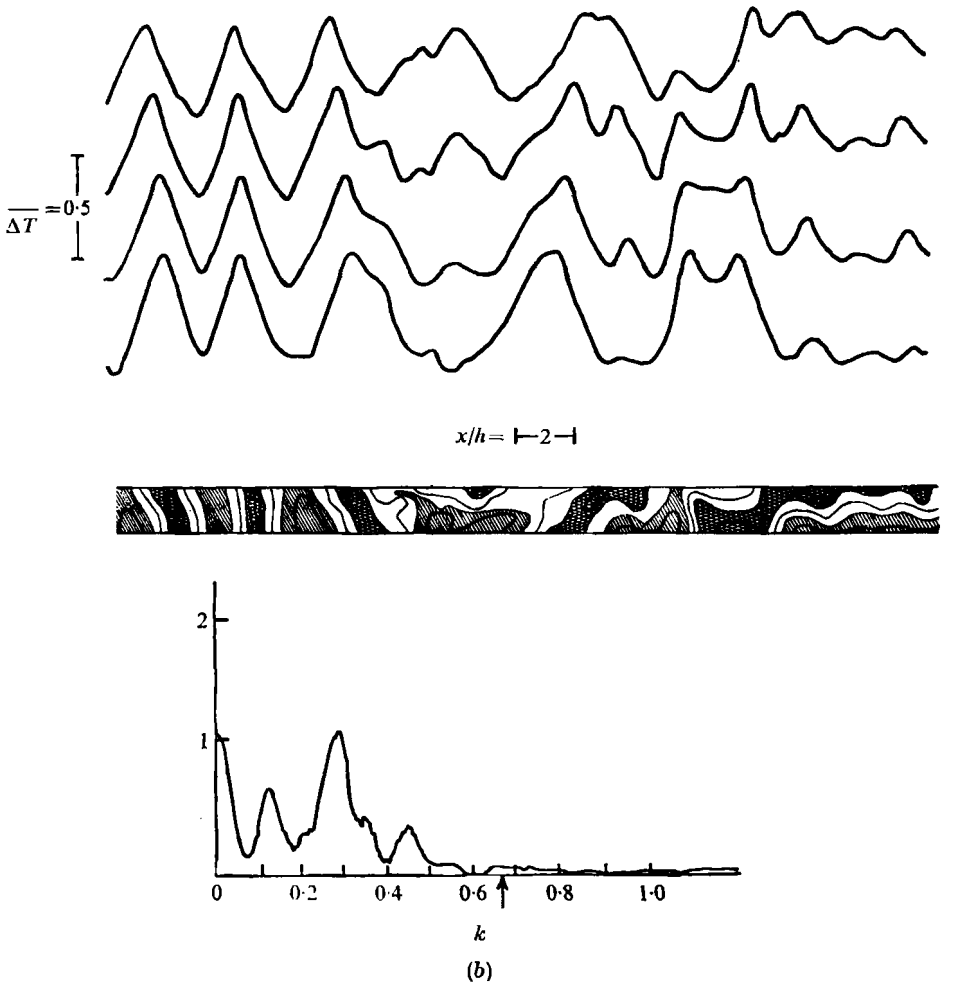

FIGURE 7. Measurements (series V) of the horizontal temperature distribution for $h = 1{\cdot}67$ cm with isotherms below. The wavenumber spectrum of the temperature fluctuations for a single trace is also shown. k is the non-dimensional cyclical wavenumber. The ordinate is an arbitrary linear energy density scale. (*a*) $Ra = 6{\cdot}09 \times 10^3$, $\Delta T = 14{\cdot}61$ °C; isotherms at non-dimensional intervals of 0·125. (*b*) $Ra = 7{\cdot}56 \times 10^3$, $\Delta T = 18{\cdot}17$ °C; isotherms at intervals of 0·110.

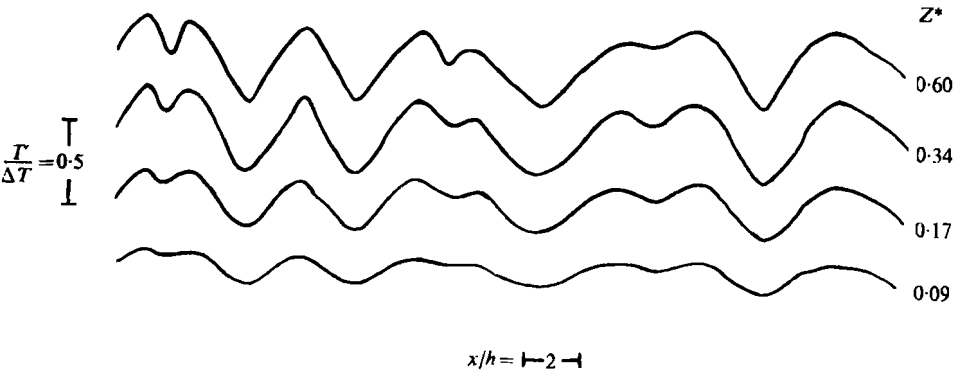

FIGURE 8. A representative measurement (series II) of the vertical temperature distribution for $Ra = 6{\cdot}7 \times 10^3$. The non-dimensional heights Z^* of each probe are shown to the right.

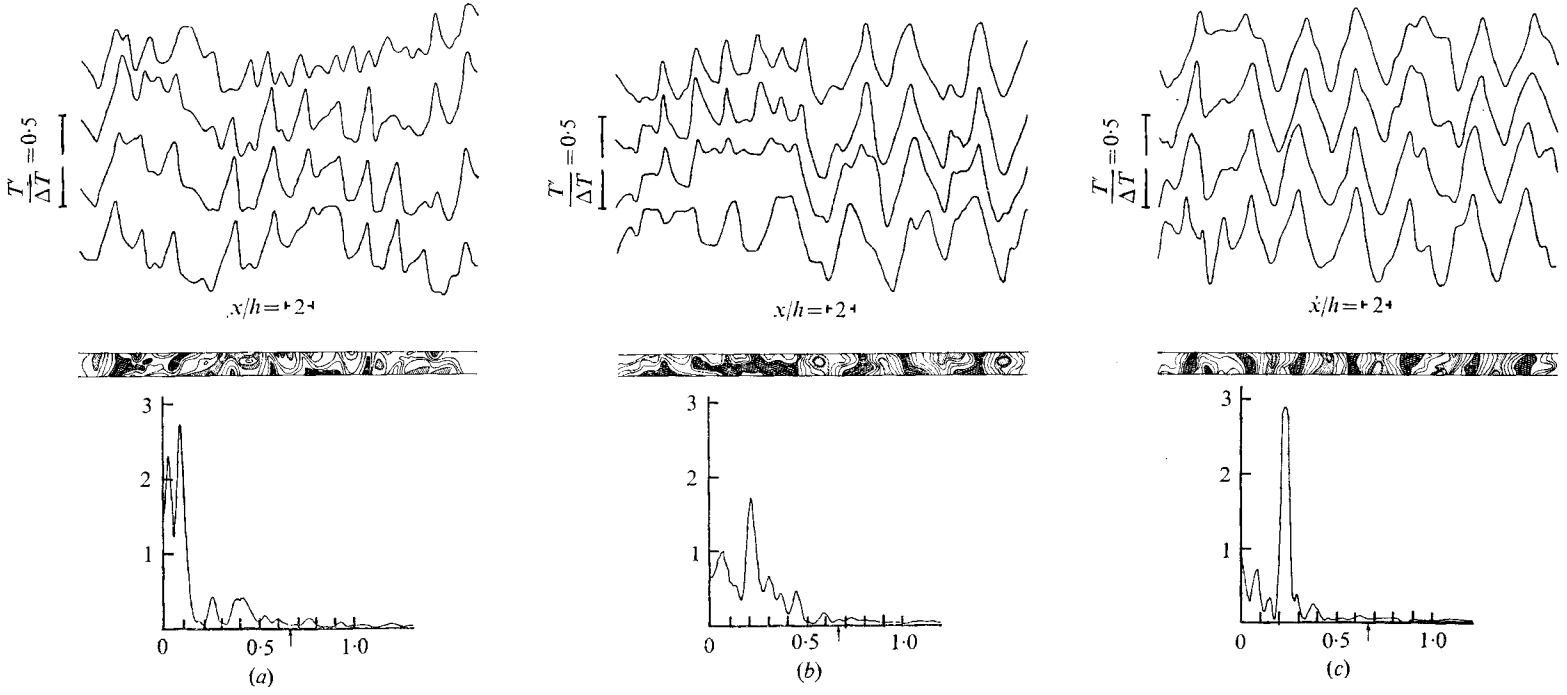

FIGURE 9. A representative group of measurements of the horizontal temperature distribution from series V for $Ra > Ra_{T_2}$. $Ra = 12 \times 10^3$, $\Delta T = 28{\cdot}90\,^{\circ}\mathrm{C}$, $h = 1{\cdot}67$ cm. The temperature measurement, isotherms and spectrum are shown for each run. The isotherms are at non-dimensional intervals of 0·07. The ordinate of the wavenumber spectrum is an arbitrary linear energy density scale. The arrow represents the non-dimensional size of the temperature probe.

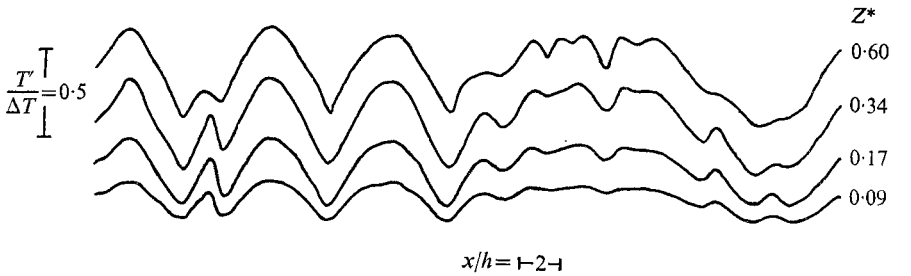

FIGURE 10. A representative measurement (series II) of the vertical temperature distribution for $Ra = 9{\cdot}45 \times 10^3$. The non-dimensional height Z^* of each probe is shown to the right.

temperature measurements is the nearly perpendicular roll orientation observed in figure 9(*c*) as compared with the skew orientations for the other two sets of measurements. The absence of the higher wavenumbers in figure 9(*c*) could be due to the probe width, which barely allows resolution of the smallest scale fluctuations ($k = 0{\cdot}65$) which were measured in figure 9(*a*). It is therefore probable that skew measurements like those in figures 9(*a*) and (*b*) are more informative about the range of horizontal scales present in the temperature field. Again, an example of vertical-array measurements, which is shown in figure 10, shows that the appearance of the temperature fluctuations is quite uniform for different heights Z_i^*.

Differences in the appearance of temperature traces made at different Z^* gradually become evident for Ra near 20×10^3. It is near these Ra that the mean temperature gradient becomes constant over a greater part of the interior region between the plates. Figures 11(*a*) and (*b*) are presented as examples of two different horizontal measurements of temperature made at different Z^* at nearly the same Ra. A comparison of these measurements with the vertical array of measurements at $Z^* = 0{\cdot}6$ and $0{\cdot}17$ which are shown in figure 11(*c*) indicates that although both horizontal-array measurements have a different appearance they could represent a similar flow configuration.

A quantitative description of the temperature distribution was obtained using analog techniques of data analysis to determine the important spatial scales of the temperature field for Ra in different heat-flux regimes. A Princeton Applied Research Correlation Function Computer and Fourier Analyzer were the main elements of a hybrid system used to calculate correlations, power spectra and cospectra of the different temperature data series, which were recorded on magnetic-tape loops. Histograms are used to summarize the spectra information from a number of temperature measurement runs (usually > 10) made at one Ra. The relative frequency with which the temperature variance exceeds a predetermined value is defined here as ϕ and is shown as a function of the non-dimensional cyclical wavenumber $k = h/\lambda$, where λ is the wavelength of the temperature fluctuation. Isotherms from a single run were used to assist in the physical interpretation of the peaks in the spectrum for that run.

The histograms shown in figure 12 represent the results of two different series of temperature measurements made at Ra values both larger and smaller than Ra_{T2}, the first supercritical heat-flux transition. Bandwidths of 0·05 were used

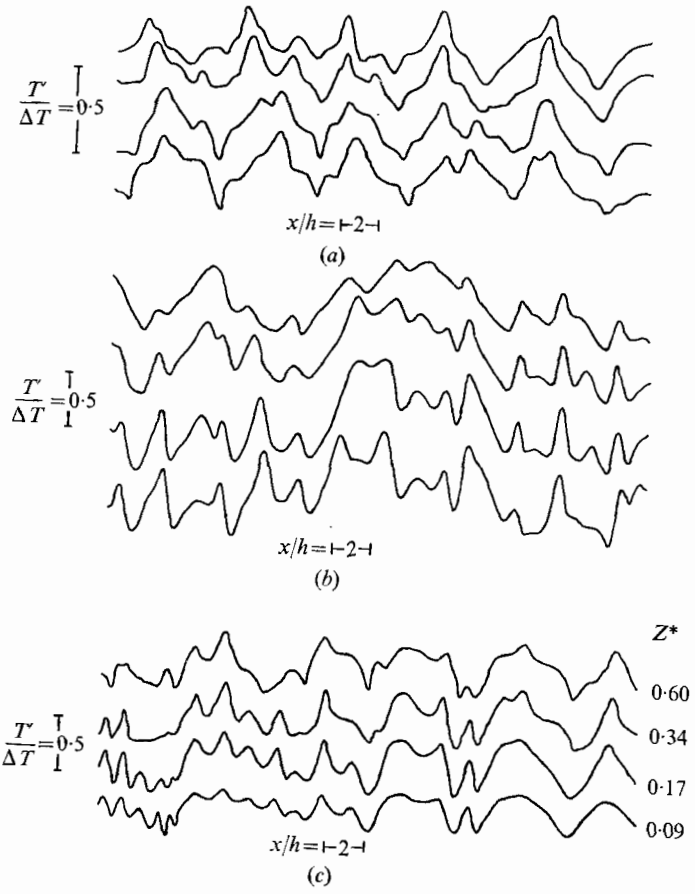

FIGURE 11. (*a*) Horizontal temperature distribution (series VII) for $Ra = 26{\cdot}8 \times 10^3$, $Z^* = 0{\cdot}42$. (*b*) Horizontal temperature distribution (series IV) for $Ra = 26{\cdot}1 \times 10^3$, $Z^* = 0{\cdot}20$. (*c*) Horizontal temperature distribution at four heights (series II), $Ra = 24{\cdot}5 \times 10^3$. Assuming symmetry in the vertical, the fluctuations at $Z^* = 0{\cdot}6$ should be comparable with those at $Z^* = 0{\cdot}4$.

for this calculation. Near $Ra = 9000$ both series exhibit a limiting wavenumber band $k = 0{\cdot}30$ above which no significant temperature variance is detected. However at both higher and lower Ra one finds temperature variance at the higher wavenumbers. The results in figure 13 show that the critical temperature variance in 0·1 bandwidths is observed at the higher wavenumbers as Ra is increased from 9700 to 47 600. The reduced resolution of the non-dimensional wavenumbers is imposed by the relatively large plate separation of $h = 2{\cdot}73$ cm for this series of measurements.

One now asks, what is the role of the changes in the horizontal wavenumber spectrum which are observed to accompany the changes in the vertical heat flux as Ra is increased from $Ra < Ra_{T2}$ to $Ra > Ra_{T2}$? The representative data samples that appear in figures 7–10 are useful aids in the interpretation of the temperature variance which is shown in the histogram at different Ra. For

$$Ra < Ra_{T2}$$

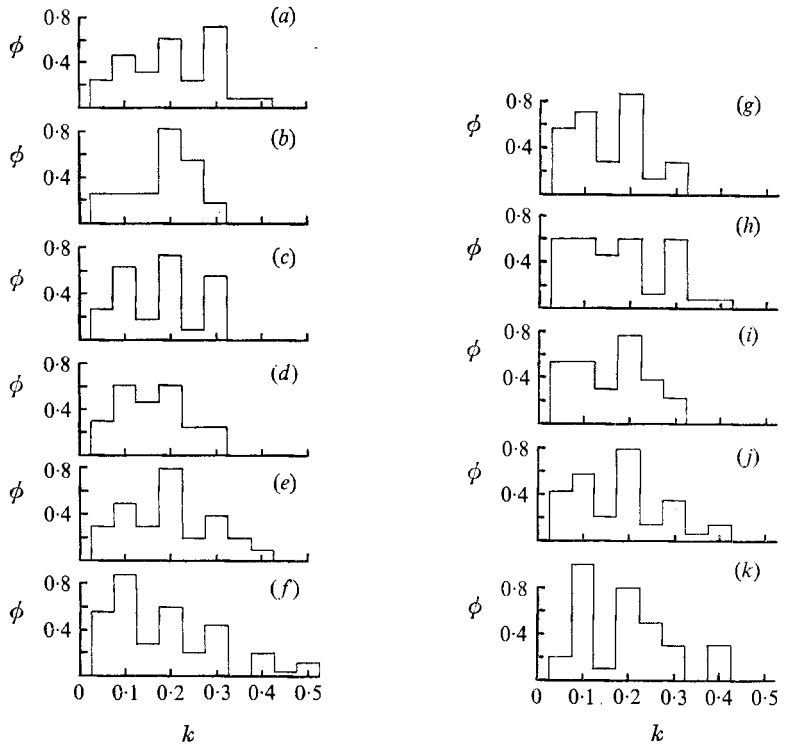

FIGURE 12. Histograms of the relative frequency of occurrence ϕ of critical temperature variance at different wavenumbers k for the $\delta\Delta T$ series III ($h = 1{\cdot}95$ cm) and V ($h = 1{\cdot}67$ cm); bandwidth = 0·05.

	Ra	ΔT (°C)	Number of runs
(*a*)	4500	10·82	13
(*b*)	6090	14·61	10
(*c*)	7560	18·17	11
(*d*)	9050	21·73	13
(*e*)	10500	25·21	10
(*f*)	1200	28·90	18
(*g*)	3900	5·58	7
(*h*)	6360	8·86	13
(*i*)	8780	12·24	13
(*j*)	11280	15·77	14
(*k*)	13900	19·47	10

it is apparent that much of the variance at $k = 0{\cdot}35$ and 0·4 in figure 12 is due to regions of roll pinching. A good example of the signature of this type of feature can be seen in figure 7 (*a*). Roll pinching has been observed by Busse & Whitehead (1971) and by Willis, Deardorff & Somerville (1972) and is described as the process which occurs in order to accommodate roll growth as Ra is increased.

There is some high wavenumber variance ($k = 0{\cdot}45$) in the right half of figure 7 (*b*), which shows an example of measurements made at $Ra = 7560$. This observation of a nearly longitudinal traverse of a roll is highly suggestive of the presence of the type of lateral waves observed by Willis & Deardorff (1970). It is note-

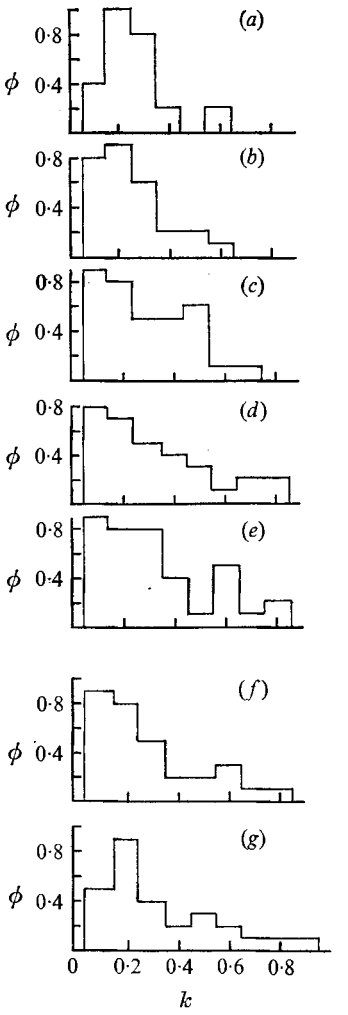

FIGURE 13. Histograms of the relative frequency of occurrence ϕ of critical temperature variance at different wavenumbers k for the $\delta\Delta T$ series IV ($h = 2{\cdot}73$); bandwidth = 1·0. The total number of runs at each Ra was 10.

	(*a*)	(*b*)	(*c*)	(*d*)	(*e*)	(*f*)	(*g*)
Ra	9830	14450	20800	26100	31750	31600	47800
ΔT (°C)	5·00	7·34	10·54	33·30	16·12	20·17	24·26

worthy that there is an absence of these waves in a similar longitudinal traverse at $Ra = 6090$ shown to the left in figure 7 (*a*). Willis & Deardorff (1970), using flow visualization techniques, observed an onset of these lateral waves at $Ra \approx 5800$. There have been no observations of a significant change in heat flux associated with the onset of this type of motion. They report that the wavenumber of these lateral waves is about 0·4 at $Ra = 9000$. Their presence confuses the interpretation of the higher wavenumber temperature fluctuations observed at $Ra > Ra_{T2}$. However, if in fact these waves have reached some equilibrium amplitude near

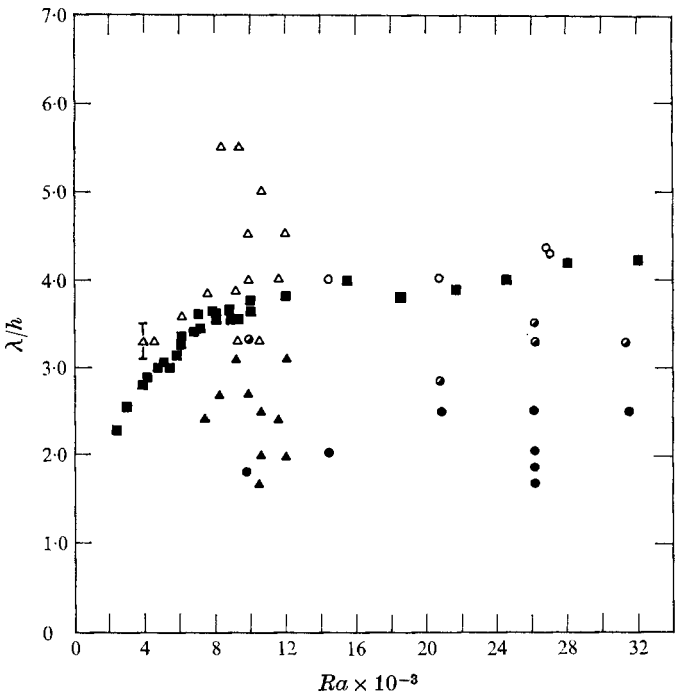

FIGURE 14. Non-dimensional wavelength λ/h of temperature fluctuations versus Ra. Uniform fluctuations: △, series V; ○, ◑, series IV. Short wavelength temperature fluctuations (see text): ▲, series V; ●, series IV. ■, average values from Willis *et al.* (1972) for comparison.

$Ra = 8000$, then their presence represents a constant amplitude noise source in the $k = 0{\cdot}4$ band (and perhaps at lower wavenumbers for the case of oblique-angle probe intersections).

For $Ra > Ra_{T2}$ the statistical presence of the double-scale temperature fluctuation which can be seen in figures 9 (*a*) and (*b*) becomes pronounced and is reflected in the histograms. The non-dimensional amplitude of these small scales nearly doubles as Ra is increased from 9000 to 12 000 and therefore presumably this is not the signature of the lateral waves observed for $Ra < Ra_{T2}$. The isotherms in figures 9 (*a*) and (*b*) suggest a pattern which is more nearly consistent with the sharp-crested waves observed by Willis & Deardorff (1970) to run intermittently along a roll edge. The asymmetry of the signature to the left in figure 9 (*b*) does not appear to be consistent with the simple form of lateral waves we observed in figure 7 (*b*). It is not clear from these measurements of such time-dependent features what relation they might have to the bimodal form of convection observed by Willis *et al.* (1972). However, these signatures are particularly distinctive for $Ra > Ra_{T2}$ because of their shape and amplitude growth. Motions represented by these signatures may play at least a partial role in changing the nature of the heat flux for $Ra > Ra_{T2}$. The measurement of the local vertical heat flux could provide the essential evidence in deciding this question.

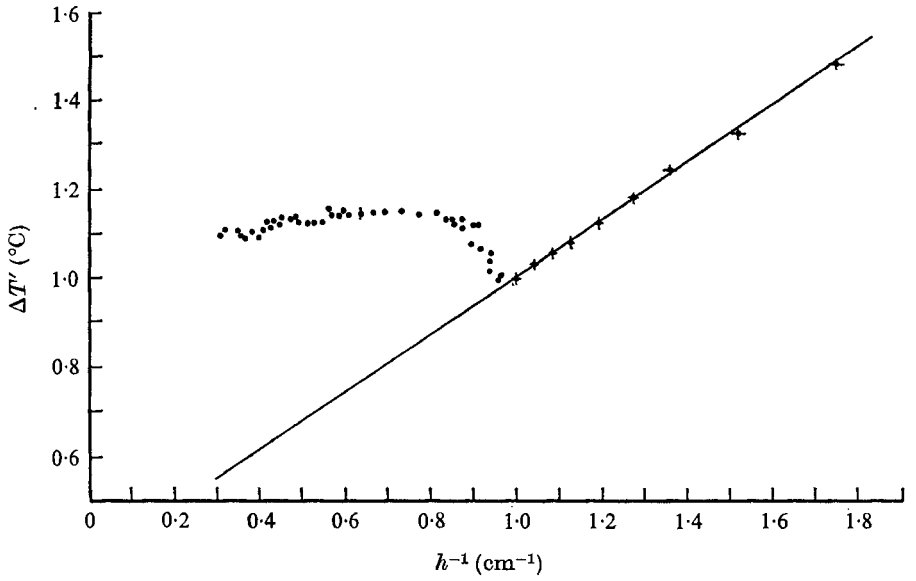

FIGURE 15. The heat-flux data for a δh series for $500 < Ra < 50\,000$ in terms of the temperature difference $\Delta T'$ across the glass plate and the inverse plate separation h^{-1}. The points used to determine the straight line are for $Ra < 1710$. Vertical and horizontal bars represent estimated errors.

One observes an increase in temperature variance at still higher wavenumbers in the histograms associated with series IV (figure 13) as Ra is increased from 9830 to 47 800. Although the peak at $k = 0{\cdot}60$ in the histograms for $Ra = 31\,750$ and 39 600 may be significant it is not conclusive evidence of the onset of an additional mode or modes near Ra_{T3}. A greater number of observations could provide the answer to that question.

An estimate of the predominate wavelength of the temperature fluctuations was made from the spectra of the more 'uniform' temperature records, figures 7 (*a*) and (*b*) and 9 (*c*) for example. The results represented by the open symbols in figure 14 are consistent with the results of Willis *et al.* (1972). However, there were some data, represented by the half-filled circles, that were just as uniform as those above and yet had systematically smaller wavelengths. The difference between the two measurements could not be accounted for by assuming different probe intersection angles.

An estimate of the wavelength of the smallest wavelength temperature fluctuation, which is represented by the closed symbols in figure 14, was made from the spectra associated with runs like those in figures 9 (*a*) and (*b*). The observed wavelengths lie in a band between 1·6 and 2·4. The scatter here probably reflects the differences in probe angle of attack. Again one would expect a larger number of measurements to produce a distribution suitable for better estimates.

In summary, this survey of temperature measurements suggests that the growth of an additional mode or modes of convection may be an important contribution to the change of slope in the observed heat flux at Ra_{T2}. Furthermore, it appears that in spite of the presence of lateral waves for Ra both greater and

less than Ra_{T_2} this means of measuring temperatures may prove useful for probing small-scale features of this type of flow. These measurements serve as a guide to new designs for probe spacings which can give a more complete picture of the temperature field. The addition of a local velocity measurement might shed some light on the coupling of the different observed modes of convection.

This paper is based on the research presented in the author's thesis at M.I.T. He is indebted to Professor Erik Mollo-Christensen for his help and advice in this investigation, which was sponsored by the Air Force Office of Scientific Research, Contract AF 49(639)-1493.

Appendix

Owing to the asymmetry of the apparatus the usual procedure of measuring temperature difference across identical heat-flux layers, above and below the working fluid, was inapplicable. For these heat-flux calculations the linear dependence of $\Delta T'$ on $1/h$ was determined in the stable regime ($Ra < Ra_{cr}$) and extrapolated into the convection regime as shown in figure 15. Then on the basis of the heat-flux balance in a simplified convection model (figure 1), in which the sum of all heat losses is represented by q_l and heat flux radiated between the plates is denoted by q_r, the Nusselt number can be found in the following way. Assuming that the total heat flux q_t passes through the glass plate we can form the balance

$$q_t = \bar{K}\Delta T' = q_c + q_v + q_r + q_l, \tag{A 1}$$

where $\bar{K}$ is the heat meter 'constant', which is in fact allowed to vary in experiments in order to compensate for heat losses and other errors. Let the quantity $\Delta T''$ denote the temperature difference across the glass plate only for a conductive heat transfer though the air (i.e. $q_v = 0$), then (A 1) becomes

$$\bar{K}\Delta T'' = q_c + q_r + q_l. \tag{A 2}$$

For the ranges of ΔT and h used empirical relationships show that q_r and q_l vary linearly with ΔT. For a δh series (ΔT constant) of measurements q_r and q_l are constant and the heat meter constant can be determined from the relation

$$\bar{K} = \frac{K_{\text{air}}\Delta T}{S}, \tag{A 3}$$

where S is the slope of $\Delta T''$ versus $1/h$ relation and the definition of conducted heat flux is

$$q_c = K_{\text{air}}\Delta T/h. \tag{A 4}$$

The convected heat flux $q_v(h^{-1})$ can be calculated from a combination of (A 1) and (A 2) according to

$$q_v = \bar{K}(\Delta T' - \Delta T''); \tag{A 5}$$

since both $\Delta T' - \Delta T''$ and S are easily determined from figure 15 and $\bar{K}$ can be found from (A 3). Note that neither a heat loss or radiation correction is directly applied

to this calculation. By substituting the results of (A 4) and (A 5) into the definition of the Nusselt number one obtains the following relation:

$$Nu - 1 = \frac{\bar{K}(\Delta T' - \Delta T'')}{(K_{\text{air}}\Delta T)/h}. \tag{A 6}$$

Heat-flux calculations using this approach were also attempted with the heat-flux data obtained from the $\delta\Delta T$ series of measurements. Owing to the combination of the scatter associated with small ΔT at low Ra and a variable radiative heat flux Nu determinations were unsatisfactory. However a useful result can be obtained from reconsidering (A 1) for the conditions of constant h and the linear dependence of q_r and q_l on ΔT, such that

$$\Delta T' = \bar{K}^{-1}[q_c + q_v + (C_1 + C_2)\,\Delta T]. \tag{A 7}$$

Using the definitions of Ra and Nu, equation (A 7) can be reorganized thus:

$$\Delta T' = \bar{K}' Nu\, Ra + \beta\, Ra, \tag{A 8}$$

where

$$\bar{K}' = \frac{K_{\text{air}}}{\alpha g h^4}\frac{\kappa\nu}{\bar{K}}, \quad \beta = \frac{C_1 + C_2}{\alpha g h^3}\kappa\nu$$

are both constants here. Because both $\partial\Delta T'/\partial Ra$ and $\partial Ra\, Nu/\partial Ra$ are proportional to Nu, slope discontinuities should occur at the same Ra in each plot, as in fact they do in the plots of $\Delta T'$ versus Ra. These plots are used to locate the heat-flux discontinuities for the $\delta\Delta T$ series.

REFERENCES

Brown, W. S. 1971 An experimental investigation of the transition to turbulence of a thermal convective flow in air between horizontal plates. Ph.D. thesis, M.I.T.

Busse, F. H. & Whitehead, J. A. 1971 Instabilities of convection rolls in a high Prandtl number fluid. *J. Fluid Mech.* **47**, 305–320.

Chen, M. M. & Whitehead, J. J. 1968 Evolution of two-dimensional periodic Rayleigh convection cells of arbitrary wave numbers. *J. Fluid Mech.* **31**, 1–15.

Chorin, A. J. 1967 Numerical study of thermal convection in a fluid layer heated from below. *J. Comp. Phys.* **2**, 1–128.

Coles, D. 1965 Transition in circular Couette flow. *J. Fluid Mech.* **21**, 385–425.

Koschmieder, E. L. 1966 On convection on a uniformly heated plane. *Beitr. Phys. Atmos.* **39**, 1–11.

Krishnamurti, R. 1970 On the transition to turbulent convection. Part 1. The transition from two- to three-dimensional flow. *J. Fluid Mech.* **42**, 295–307.

Malkus, W. V. R. 1954 Discrete transitions in turbulent convection. *Proc. Roy. Soc.* A **225**, 196–212.

Schmidt, R. J. & Milverton, S. W. 1935 On the stability of a fluid when heated from below. *Proc. Roy. Soc.* A **152**, 586–594.

Silveston, P. L. 1958 Warmed urchgang in waagerechten Flussigkeitsschichten. *Forsch. Gebeite Ingenieurw.* **24**, 59–69.

Willis, G. E. & Deardorff, J. W. 1967 Confirmation and renumbering of the discrete heat flux transitions of Malkus. *Phys. Fluids*, **10**, 1861–1866.

Willis, G. E. & Deardorff, J. W. 1970 The oscillatory motions of Rayleigh convection. *J. Fluid Mech.* **44**, 661–672.

Willis, G. E., Deardorff, J. W. & Somerville, R. C. J. 1972 Roll-diameter dependence in Rayleigh convection and its effect upon heat flux. *J. Fluid Mech.* **54**, 351–368.